Determination of flow directions by combining AMS and thin-section analyses: implications for Oligocene volcanism in the Kerguelen Archipelago (southern Indian Ocean)

G Plenier, P Camps, Benoît Henry, B Ildefonse

Geophys. J. Int. (2005) **160,** 63–78 doi: 10.1111/j.1365-246X.2004.02488.x

Determination of flow directions by combining AMS and thin-section analyses: implications for Oligocene volcanism in the Kerguelen Archipelago (southern Indian Ocean)

G. Plenier,[1,*] P. Camps,[2] B. Henry[3] and B. Ildefonse[2]

[1] *Laboratoire Géophysique, Tectonique et Sédimentologie, CNRS and ISTEEM, Université Montpellier* 2 *case* 060, 34095 *Montpellier Cedex* 05, *France*
[2] *Laboratoire de Tectonophysique, CNRS and ISTEEM, Université Montpellier* 2 *case* 049, 34095 *Montpellier Cedex* 05, *France. E-mail: camps@dstu.univ-montp2.fr*
[3] *Géomagnétisme et Paléomagnétisme, CNRS and IPGP,* 4 *Avenue de Neptune,* 94107 *Saint-Maur Cedex, France*

Accepted 2004 September 20. Received 2004 September 20; in original form 2003 February 19

SUMMARY

We report an anisotropy of magnetic susceptibility (AMS) study carried out on seven Oligocene volcanic sections widely distributed on the surface of the Kerguelen Archipelago. The statistical results at flow scale and at section scale were checked with AMS density diagrams and thin-section analysis. Because of the axis permutations frequently observed for lava flows, two possible flow directions were nicely defined for the majority of the sections. We then used two alternative approaches (imbrication of the minimum axis and symmetry of the AMS distribution) to infer a flow direction for each section. These two methods and thin-section analysis not being decisive for choosing between the two solutions, geological and geomorphological observations were finally used to obtain confident interpretations. The results of this study enable the supposed eruptive centres of the Kerguelen Archipelago to be located more precisely.

Key words: anisotropy, Kerguelen Archipelago, lava flows, magnetic susceptibility, shape preferential orientation.

1 INTRODUCTION

The magnetic susceptibility of a rock is a function of the minerals present and of their individual characteristics. It generally displays a directional variability referred to as the anisotropy of magnetic susceptibility (AMS). The AMS is represented by a second-rank tensor of eigenvectors K_{min}, K_{int} and K_{max} (Hrouda 1982; Borradaile 1988; Rochette *et al.* 1992; Tarling & Hrouda 1993; Borradaile & Henry 1997; Bouchez 2000). For undeformed volcanic rocks, the global AMS is usually controlled by the presence of titanomagnetites, and reflects either their anisotropy of distribution, after they belatedly crystallized in interstitial zones within the pre-existing silicate phase during lava flow (Hargraves *et al.* 1991), or more directly their orientation acquired during emplacement (Hrouda 1982; Cañón Tapia *et al.* 1995; Morris 2000). In each case, the AMS records the end of flow emplacement (Ventura 2001). Usually, the anisotropy of magnetic susceptibility is weak, suggesting a not very effective orientation mechanism. This should be particularly true for lava flows, where conditions of magma emplacement are less constrained than for dyke intrusions. Indeed, the absence of a second solid surface on the roof of the lavas during emplacement may prevent the magma flux from stabilizing. Moreover, the underlying surface, affected by erosion and/or tectonics (faults, folds, etc.) or the roof of a previous flow, is generally less planar than dyke walls, and the magma flux can therefore easily be diverted by natural obstacles. The magnetic lineation (K_{max}) is found to be either parallel or perpendicular to the flow direction (Cañón Tapia *et al.* 1995; Glen *et al.* 1997; Morris 2000; Herrero-Bervera *et al.* 2002; Henry *et al.* 2003), even for samples from the same flow. The magnetic foliation (pole given by K_{min}), on the other hand, is often close to the flow plane (Kolofikova 1976; Cañón Tapia *et al.* 1996). By analogy with the use of imbrication to determine the flow sense within a dyke (Knight & Walker 1988; Tauxe *et al.* 1998; Geoffroy *et al.* 2002), AMS was also proposed to infer the flow sense within a lava flow (Cañón Tapia *et al.* 1997). In this paper, the flow direction refers to the azimuth of flow and the flow sense to the way it flows (from N to S for example).

Two previous AMS studies have been carried out in the Kerguelen Archipelago. Plenier *et al.* (2002) aimed to determine if the dip observed at a section was due either to an initial topography existing before the lava emplacement or to a late tectonic tilting of the whole sequence. They found a flow direction parallel to the dip of the lava pile, and thus did not apply a tilt correction to their palaeomagnetic data for this section. Henry *et al.* (2003) detected some variations of emplacement conditions along another section presenting a thick interbedded conglomerate layer. Their analysis revealed a weak tilting in the southeastern part of the Archipelago.

*Now at: Department of Earth Science, University of California, Santa Cruz, CA 95064, USA.

In both studies the principal susceptibility directions displayed numerous permutations, even at flow scale, but flow directions were confidently defined.

The principal aim of this study is to determine the emplacement directions in seven sections distributed on the surface of the Archipelago in order to localize their respective eruptive centres [see Zhu *et al.* (2003) for a comparable study on Hannuoba basalts, northern China]. We present three different but complementary approaches for interpreting the AMS measurements: analysis at the section scale, at the flow scale, and using density diagrams. Owing to the frequent permutations, thin-section analysis is also used to check the reliability of the flow directions obtained by AMS studies. Finally, the interpreted flow sense will be compared with that proposed by Nougier (1970a) from field observations (present dip, thickness variation and fault distribution of the lava piles).

2 GEOLOGY AND SAMPLING

The Kerguelen Archipelago (Nougier 1970a; Giret 1986) is located at 70°E, 49°S in the southern Indian Ocean, on the northern part of the Kerguelen–Gaussberg Plateau. It represents the aerial continuation of the Kerguelen plume magmatic activity over the last 30 Myr (Yang *et al.* 1998; Weis *et al.* 1998; Nicolaysen *et al.* 2000). Some magmatic contributions related to the Southeast Indian Ridge during the early Cenozoic are also suspected (Doucet *et al.* 2002). Lava flows are preponderant in the Archipelago. They crop out on more than 85 per cent of the surface and form 400 to 900 m high tabular relief incised by glacial erosion. Gabbro, granite and syenite intrusions from 1 to 15 km in diameter are also present locally. These plutons, derived from later Kerguelen plume melts (Giret 1990; Weis & Giret 1994), compose with a few sediments the rest of the rocks cropping out in the archipelago.

First, about seven samples per flow, oriented using magnetic and solar compasses, were collected in order to measure palaeosecular variation and palaeointensity (Plenier *et al.* 2002, 2003). All the successive least-altered lava flows (1 to 10 m thick) were sampled in their bottom part, which generally gives the most reliable indication for flow direction from AMS studies (Glen *et al.* 1997; Herrero-Bervera *et al.* 2002). The collected lavas are equally distributed throughout each section and are thus representative of the lava piles. The samples were collected as far as possible from dykes, and close to previously dated sections (Yang *et al.* 1998; Nicolaysen *et al.* 2000; Doucet *et al.* 2002), namely across Sections 1 (Port Christmas: 16 flows), 2 (Mont des Ruches: 18 flows), 3 (Mont des Tempêtes: 20 flows), 4 (Port Couvreux: 6 flows), 5 (Mont Amery: 8 top flows), 6 (Port Raymond : 9 flows) and 7 (Mont Bureau : 18 flows) (Fig. 1). For Section 5, we completed our sampling with about 50 samples, previously collected by Henry & Plessard (1997), from the eight

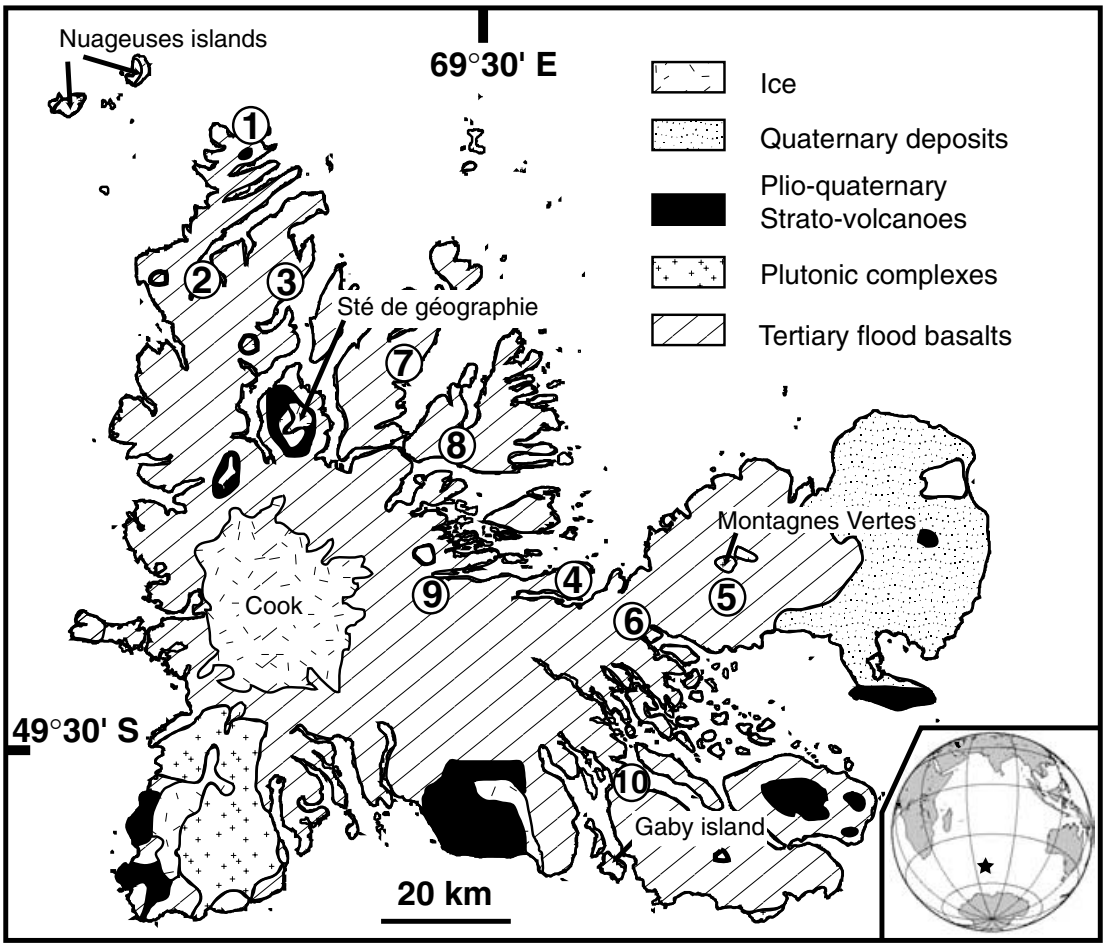

Figure 1. Geological map of the Kerguelen Archipelago after Frey *et al.* (2000). Numbers indicate the locations of sampled sections: (1) Port Christmas : 16 flows, (2) Mont des Ruches : 18 flows, (3) Mont des Tempêtes : 20 flows, (4) Port Couvreux : 6 flows, (5) Mont Amery : 16 flows, (6) Port Raymond : 9 flows and (7) Mont Bureau : 18 flows. Other studied sections: (8) Mont de la Rabouillère (Plenier *et al.* 2004), (9) Mont de la Tourmente (Plenier *et al.* 2002) and (10) Port Jeanne d'Arc (Henry *et al.* 2003).

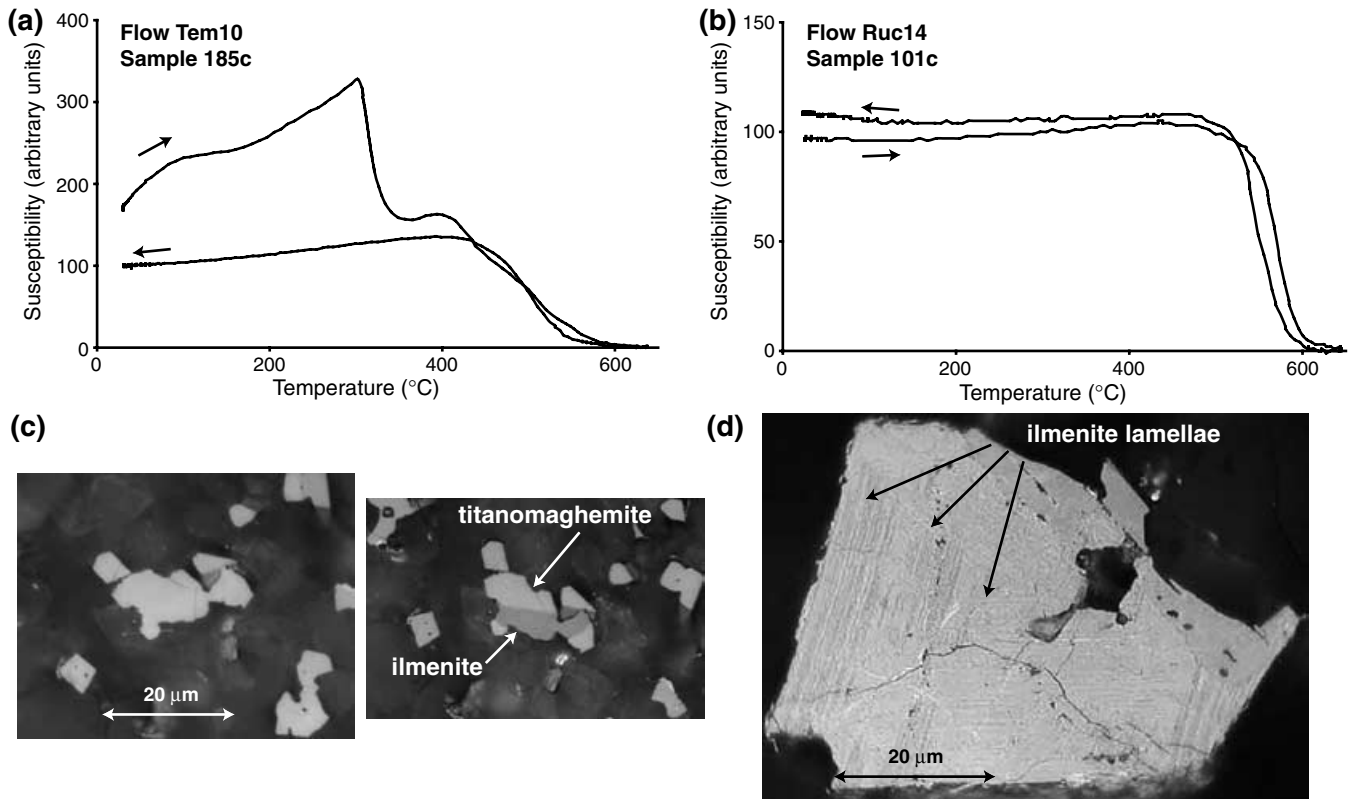

Figure 2. (a) and (b) Representative *K–T* curves of irreversible and reversible behaviour respectively. (c) and (d) Associated reflected light microphotographs using an oil immersion lens: (c) natural light with different orientations, and (d) in polarized light.

bottom flows just below (VA-VH). No significant dip was observed for these lava sequences, except for sections 4 and 6, for which dips of 5° E and of 4° ESE were measured, respectively.

3 ROCK MAGNETISM

The magnetic carriers of one sample per flow for Sections 2, 3 and 4 were identified (Plenier *et al.* 2003) using low-field susceptibility thermal evolution curves (*K–T* curves). Two distinct behaviours were observed. Irreversible and complex *K–T* curves correspond to an assembly of original rich-Ti titanomagnetites or slightly oxidized titanomaghemites with higher-Curie-temperature titanomaghemites resulting from low-temperature oxidation (Fig. 2a). Reversible *K–T* curves characterize poor-Ti titanomagnetites produced by high-temperature oxyexsolution of the original titanomagnetite during the flow emplacement (Fig. 2b). Thin-section observation with an oil immersion lens gave similar conclusions. We found samples showing irreversible *K–T* curves to be associated with pleochroic ilmenite and an optically isotropic phase interpreted as a titanomaghemite (Fig. 2c). For samples presenting reversible *K–T* curves, exsolved ilmenite or titanohematite lamellae result from deuteric oxidation of a residual titanomagnetite (Fig. 2d).

4 ANISOTROPY OF MAGNETIC SUSCEPTIBILITY

The AMS of 649 non-demagnetized standard samples was measured using KLY2 and KLY3 Kappabridges at IPGP (Saint Maur) and Montpellier palaeomagnetic laboratories respectively. Owing to the occurrence of conglomerate at the base of the third flow from the Mont des Ruches section (Section 2) and the low numbers of samples (8) in the underlying units, these two bottom flows have been rejected from the rest of the analysis. Indeed, they may have experienced different emplacement conditions (in particular taking place with different dips), as previously observed in the analysis of the Port Jeanne d'Arc section (Henry *et al.* 2003). They need therefore to be discarded. In the end, 641 samples were kept for the determination of flow direction.

The data have been analysed at two different scales to determine the flow direction. In each case, the confidence zone for the mean direction of each axis was calculated using both linear perturbation analysis (Hext 1963; Jelinek 1978; Lienert 1991) and the bootstrap method (Constable & Tauxe 1990). These two statistics provide approximately the same results, so only the bootstrap ellipses are displayed in the figures.

4.1 Flow-scale analysis

In this approach, we first calculated the mean directions of the principal susceptibilities for each individual flow and then averaged them to estimate the mean directions of the section as a whole. Lava flows with less than four samples and those for which the principal susceptibility directions were poorly defined (displaying two or three principal directions that were not statistically different) were excluded from the analysis.

The relatively low number of samples per flow is probably the main reason for the low percentage (less than 50 per cent) of flows that yielded reliable results (Table 1). This problem was previously pointed out by Cañón Tapia *et al.* (1997), who concluded that measurement of less than 10 specimens per flow often yields a large statistical uncertainty for the susceptibility principal directions.

Table 1. Summary of anisotropy of magnetic susceptibility results from the lava-flow-scale study. n/N is the number of samples per data set/total number of samples collected or the number of flows used/total number of flows collected. K_{mean} is the mean volume susceptibility ($\times 10^{-3}$). $\bar{s}$ is the eigenvalue of the normalized mean susceptibility tensor. Dec and Inc are the declination and the inclination of the mean susceptibility axes, respectively. E2:E1 are the semi-angles of the minor and major axes, respectively, of the 95 per cent confidence ellipse determined using the bootstrap statistic (Constable & Tauxe 1990). P' and T are the corrected degree of anisotropy and the shape-factor parameter, respectively (Jelinek 1981). The lava flows are labelled upwards.

Flow	n/N	K_{mean}		$\bar{s}$	Dec	Inc	E2:E1	P'	T
			Section 1 (Port Christmas: 48.67°S, 69.02°E)						
ca1	7/7	10.8	Max	1.009	292.5	1.9	7.7/9.4	1.018	−0.11
			Int	0.999	23.4	24.7	9.3/18.3		
			Min	0.992	198.3	65.3	5.6/19.5		
ca2	7/7	11.7	Max	1.004	112	17.2	5.6/36.7	1.007	−0.04
			Int	1.000	18.4	11.5	29.4/35.3		
			Min	0.996	256.1	69.1	12.2/27.9		
ca3	6/7	11.4	Max	1.003	292.4	6.8	11.7/73.2	1.008	0.57
			Int	1.001	202.0	3.9	23.3/85.3		
			Min	0.995	82.7	82.2	12.5/25.0		
ca6	7/7	8.4	Max	1.008	330.3	1.7	8.3/20.8	1.015	−0.10
			Int	0.999	60.7	15.0	16.0/21.0		
			Min	0.993	234.0	74.9	7.9/16.6		
ca7	7/7	8.5	Max	1.007	209.5	21.7	8.1/30.5	1.016	0.10
			Int	1.000	300.1	1.6	26.5/37.8		
			Min	0.992	34.1	68.2	8.8/34.6		
ca14	7/7	14.5	Max	1.003	320.5	11.9	8.8/12.9	1.007	0.31
			Int	1.001	219.2	42.8	10.6/20.1		
			Min	0.996	62.6	44.8	8.6/21.0		
ca16	7/7	12.9	Max	1.009	160.9	1.3	6.5/21.3	1.020	0.18
			Int	1.001	251.4	19.6	9.3/21.2		
			Min	0.990	67.3	70.3	6.3/9.4		
Whole section	7/16	11.0	Max	1.005	320.4	1.1	6.1/23.8	1.010	0.28
			Int	1.001	230.3	7.6	9.5/24.4		
			Min	0.995	58.3	82.4	5.9/10.8		
			Section 2 (Mont des Ruches: 48.87°S, 68.91°E)						
Ruc6	8/8	14.1	Max	1.016	164.9	7.0	8.3/14.7	1.031	−0.19
			Int	0.998	257.8	22.5	8.9/14.1		
			Min	0.986	58.7	66.3	11.9/16.4		
Ruc8	8/8	14.2	Max	1.022	148.9	9.5	10.2/79.4	1.064	0.72
			Int	1.014	240.8	11.2	13.2/83.1		
			Min	0.965	19.6	75.3	8.4/14.5		
Ruc9	9/11	31.9	Max	1.014	164.0	12.4	10.0/21.8	1.025	−0.36
			Int	0.997	65.5	33.6	20.8/44.9		
			Min	0.989	271.3	53.5	11.8/43.6		
Ruc12	7/7	28.4	Max	1.015	123.9	20.0	7.8/16.4	1.032	0.10
			Int	1.001	30.4	9.6	15.8/31.6		
			Min	0.984	276.2	67.6	7.2/32.3		
Ruc13	7/7	29.6	Max	1.017	123.2	20.2	14.9/90.0	1.033	−0.13
			Int	0.999	216.6	9.1	31.6/90.0		
			Min	0.985	329.6	67.7	22.0/38.0		
Ruc14	6/7	15.7	Max	1.017	197.1	58.7	10.9/33.2	1.034	−0.03
			Int	1.000	320.8	18.6	14.9/43.4		
			Min	0.983	59.5	24.2	13.1/28.8		
Ruc15	6/7	8.4	Max	1.015	230.9	19.0	11.1/49.8	1.040	0.52
			Int	1.006	140.9	0.1	10.0/48.5		
			Min	0.978	50.7	71.0	10.6/17.5		

Table 1. (*Continued.*)

Flow	n/N	K_{mean}		$\bar{s}$	Dec	Inc	E2:E1	P'	T
Whole section	7/18	18.5	Max	1.013	155.2	14.1	7.2/21.5	1.028	0.20
			Int	1.002	247.6	9.6	11.5/22.7		
			Min	0.986	10.7	72.9	7.0/13.2		
			Section 3 (Mont des Tempêtes: 48.88°S, 69.11°E)						
Temp1	6/7	17.5	Max	1.017	162.4	12.5	7.5/27.0	1.050	0.69
			Int	1.010	254.9	11.1	6.9/27.1		
			Min	0.972	25.2	73.2	4.9/8.8		
Temp4	7/7	4.1	Max	1.004	327.4	1.0	15.5/26.5	1.008	−0.08
			Int	1.000	57.6	15.4	22.8/44.0		
			Min	0.996	233.8	74.6	14.7/42.6		
Temp6	5/5	3.3	Max	1.001	18.5	8.5	26.0/53.4	1.003	0.23
			Int	1.000	109.4	6.3	27.3/53.8		
			Min	0.998	235.6	79.4	21.5/31.7		
Temp11	7/7	16.8	Max	1.009	200.0	9.8	31.6/42.5	1.018	0.07
			Int	1.000	290.7	4.1	34.9/41.9		
			Min	0.991	42.8	79.3	33.3/35.4		
Temp12	7/7	9.9	Max	1.022	184.8	3.3	11.0/90.0	1.046	0.12
			Int	1.002	93.4	23.5	37.1/90.0		
			Min	0.977	282.4	66.3	11.7/46.1		
Temp17	7/7	19.2	Max	1.003	163.6	8.4	20.8/62.6	1.007	0.25
			Int	1.001	70.7	19.2	25.6/68.3		
			Min	0.996	276.1	68.9	23.7/37.8		
Temp18	8/8	13.4	Max	1.006	337.4	8.2	11.6/22.7	1.011	−0.24
			Int	0.999	243.2	27.1	22.7/43.6		
			Min	0.995	82.8	61.5	11.9/42.7		
Temp20	8/8	6.0	Max	1.028	167.6	14.3	10.4/11.6	1.050	−0.51
			Int	0.992	275.5	50.4	13.0/44.5		
			Min	0.981	66.9	36.0	9.0/45.4		
Whole section	8/20	9.8	Max	1.011	171.2	9.3	6.9/18.3	1.021	−0.15
			Int	0.999	261.7	3.2	14.1/21.5		
			Min	0.990	10.4	80.1	7.1/17.8		
			Section 5 (Mont Amery: 49.29°S, 70.06°E)						
VA	6/6	53.3	Max	1.024	84.3	25.7	15.0/16.6	1.044	−0.41
			Int	0.994	334.4	35.2	16.8/55.8		
			Min	0.982	201.8	43.8	13.0/57.2		
VE	6/6	33.1	Max	1.011	15.3	6.2	13.5/62.0	1.029	0.58
			Int	1.005	281.2	32.9	24.4/65.2		
			Min	0.984	114.8	56.4	12.4/24.5		
VF	6/6	25.2	Max	1.017	10.3	2.2	11.1/30.8	1.040	0.30
			Int	1.004	279.9	9.6	17.3/33.8		
			Min	0.979	113.3	80.2	8.5/21.2		
Ame3	7/7	51.4	Max	1.025	346.8	10.5	6.1/19.3	1.069	0.64
			Int	1.013	79.9	16.2	7.2/20.3		
			Min	0.962	225.1	70.5	6.1/9.3		
Ame4	7/7	23.5	Max	1.028	149.7	62.2	14.5/18.1	1.053	−0.35
			Int	0.994	328.2	27.8	12.6/45.0		
			Min	0.978	58.6	0.6	13.9/42.6		
Ame5	7/7	23.2	Max	1.018	329.0	11.5	10.3/26.1	1.033	−0.31
			Int	0.997	61.0	9.6	23.6/34.2		
			Min	0.986	189.8	75.0	12.0/33.1		

Table 1. (*Continued.*)

Flow	n/N	K_{mean}		$\bar{s}$	Dec	Inc	E2:E1	P'	T
Ame6	7/7	14.8	Max	1.021	151.9	8.1	5.1/11.6	1.041	−0.25
			Int	0.997	14.9	79.0	11.7/25.5		
			Min	0.982	243.0	7.4	4.6/25.6		
Ame7	5/7	31.4	Max	1.032	163.7	0.7	4.3/7.9	1.061	−0.29
			Int	0.994	253.8	7.3	4.3/21.0		
			Min	0.974	68.5	82.7	6.6/21.1		
Ame8	7/7	24.2	Max	1.011	315.7	9.4	8.2/12.8	1.024	0.25
			Int	1.002	222.2	20.4	7.1/13.2		
			Min	0.987	69.2	67.3	7.0/13.2		
Whole section	9/16	28.4	Max	1.012	334.0	2.3	7.0/14.1	1.022	0.34
			Int	0.998	64.5	13.7	13.6/29.5		
			Min	0.990	234.6	76.1	7.0/29.0		
				Section 6 (Port Raymond: 49.34°S, 69.80°E)					
ra2	7/7	22.6	Max	1.026	110.1	5.6	1.7/5.3	1.047	−0.56
			Int	0.992	15.4	39.8	1.8/16.5		
			Min	0.982	206.7	49.7	5.2/16.5		
ra3	7/7	50.7	Max	1.023	114.8	0.3	8.3/28.2	1.052	0.30
			Int	1.005	204.9	20.4	29.8/46.9		
			Min	0.973	24.0	69.6	7.9/45.9		
ra5	7/7	69.7	Max	1.028	113.9	8.7	7.6/10.7	1.050	−0.62
			Int	0.990	13.6	49.3	10.0/56.6		
			Min	0.982	211.1	39.3	9.1/56.6		
ra6	7/7	52.6	Max	1.026	274.5	2.2	10.4/32.9	1.070	0.60
			Int	1.012	183.6	23.6	13.7/31.9		
			Min	0.962	9.5	66.3	6.9/17.1		
ra7	7/7	42.4	Max	1.012	278.1	13.6	11.4/43.1	1.033	0.561
			Int	1.006	181.1	26.9	15.5/44.7		
			Min	0.982	32.2	59.3	13.3/18.4		
ra8	7/7	40.4	Max	1.018	272.6	10.2	7.0/14.0	1.044	0.38
			Int	1.005	175.4	34.8	4.4/14.2		
			Min	0.976	16.6	53.3	5.4/7.7		
ra9	7/7	42.7	Max	1.015	146.2	14.5	19.2/59.3	1.030	0.06
			Int	1.000	55.8	1.6	23.6/60.0		
			Min	0.985	319.7	75.4	17.4/24.6		
Whole section	7/9	44.1	Max	1.020	112.1	3.5	4.8/7.8	1.040	0.02
			Int	1.000	203.5	22.4	7.8/98		
			Min	0.980	13.7	67.3	4.8/9.8		
				Section 7 (Mont Bureau: 48.97°S, 69.35°E)}					
fa3	5/7	27.2	Max	1.013	36.0	27.2	9.2/31.3	1.033	0.53
			Int	1.005	295.8	19.0	13.6/32.0		
			Min	0.982	175.3	55.9	7.4/16.2		
fa6	4/7	46.1	Max	1.014	348.4	40.9	9.9/31.6	1.028	0.04
			Int	1.000	249.0	10.6	20.3/36.5		
			Min	0.986	147.4	47.2	23.6/33.1		
fa7	5/7	6.4	Max	1.021	219.0	18.4	1.8/13.0	1.037	−0.65
			Int	0.993	313.4	13.1	13.1/45.0		
			Min	0.987	77.0	67.1	3.3/44.9		
fa8	4/7	37.0	Max	1.021	229.2	19.8	7.5/21.5	1.039	−0.40
			Int	0.995	137.4	5.0	20.2/87.6		
			Min	0.984	33.9	69.5	9.5/76.5		

Table 1. (*Continued.*)

Flow	n/N	K_{mean}		$\bar{s}$	Dec	Inc	E2:E1	P'	T
fa10	6/7	14.3	Max	1.014	255.3	15.6	14.3/65.0	1.037	0.50
			Int	1.006	350.0	16.4	25.1/63.7		
			Min	0.980	124.1	67.1	15.7/23.1		
Whole section	5/18	19.7	Max	1.012	231.5	7.4	11.7/24.5	1.026	0.24
			Int	1.002	325.3	26.7	14.6/24.8		
			Min	0.986	127.3	62.1	10.1/16.0		

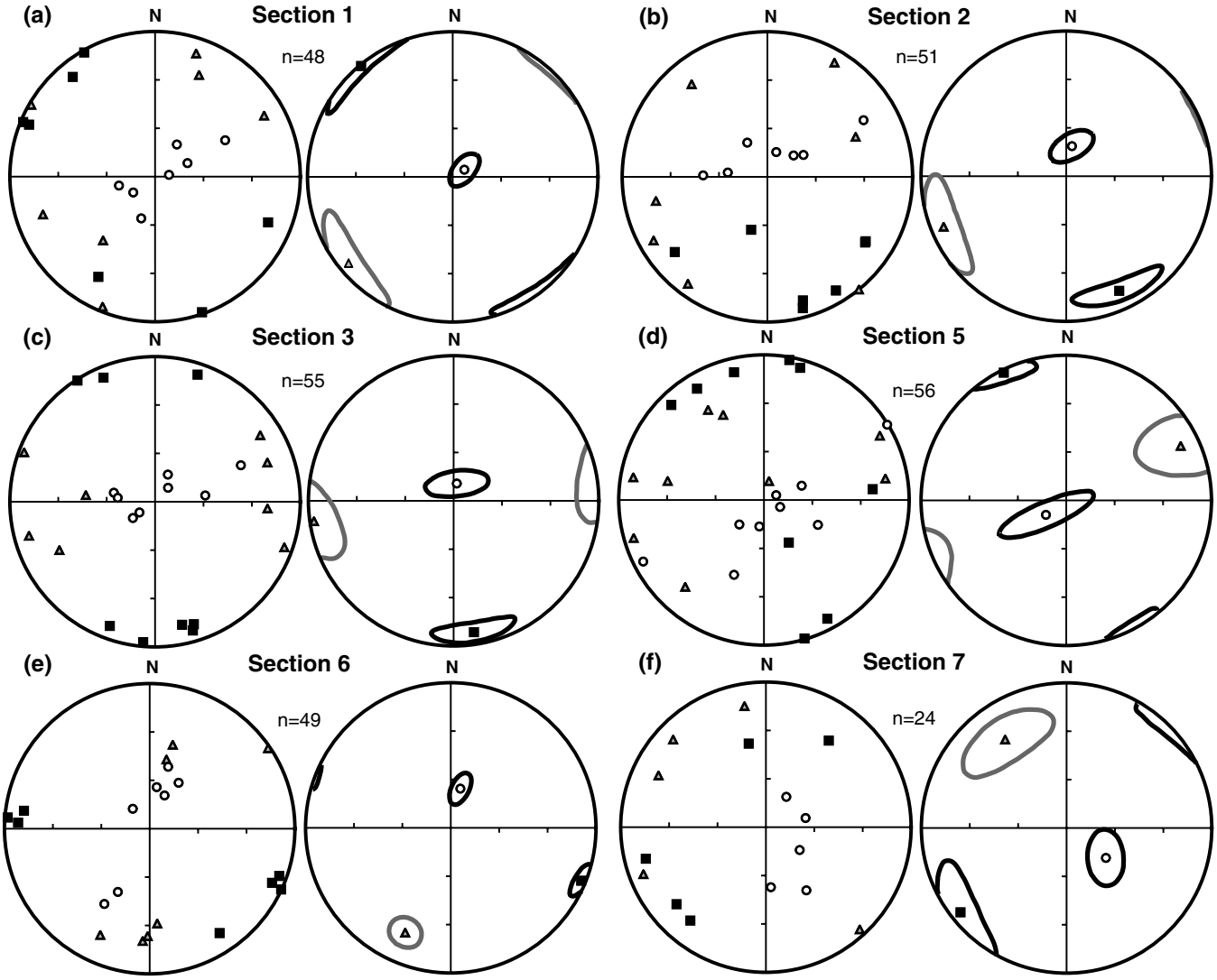

Figure 3. Flow-scale analysis: left, mean principal axes of the suitable flows; right, resulting mean principal axes of each section and their 95 per cent confidence ellipses (Constable & Tauxe 1990). Black squares K_{max}, grey triangles K_{int}, and white circles K_{min}. The equal-area projections are lower hemispheres in geographic coordinates.

With only two remaining flows, Section 4 was not subjected to further analysis. For the other six sections, however, the mean directions of the selected flows are relatively well grouped (left part of Fig. 3), and allow the determination of a mean magnetic fabric representative of each lava pile (Table 1 and right part of Fig. 3).

The three northern sections (Sections 1, 2 and 3), and Sections 5 and 6 present a very similar magnetic fabric: K_{max} is almost horizontal with a direction between N–S and NW–SE, and K_{min} is close to vertical. For Section 7, this fabric changes slightly, with K_{max} oriented SW–NE. Confidence zones are of variable size. The confidence ellipse for K_{min} is elongated in a plane perpendicular to K_{max}, whereas it is elongated in the horizontal plane (perpendicular to K_{min}) for K_{max}.

4.2 Grouping of the flows

The flow-scale analysis led to the rejection of more than half of the studied flows and did not allow any interpretation concerning

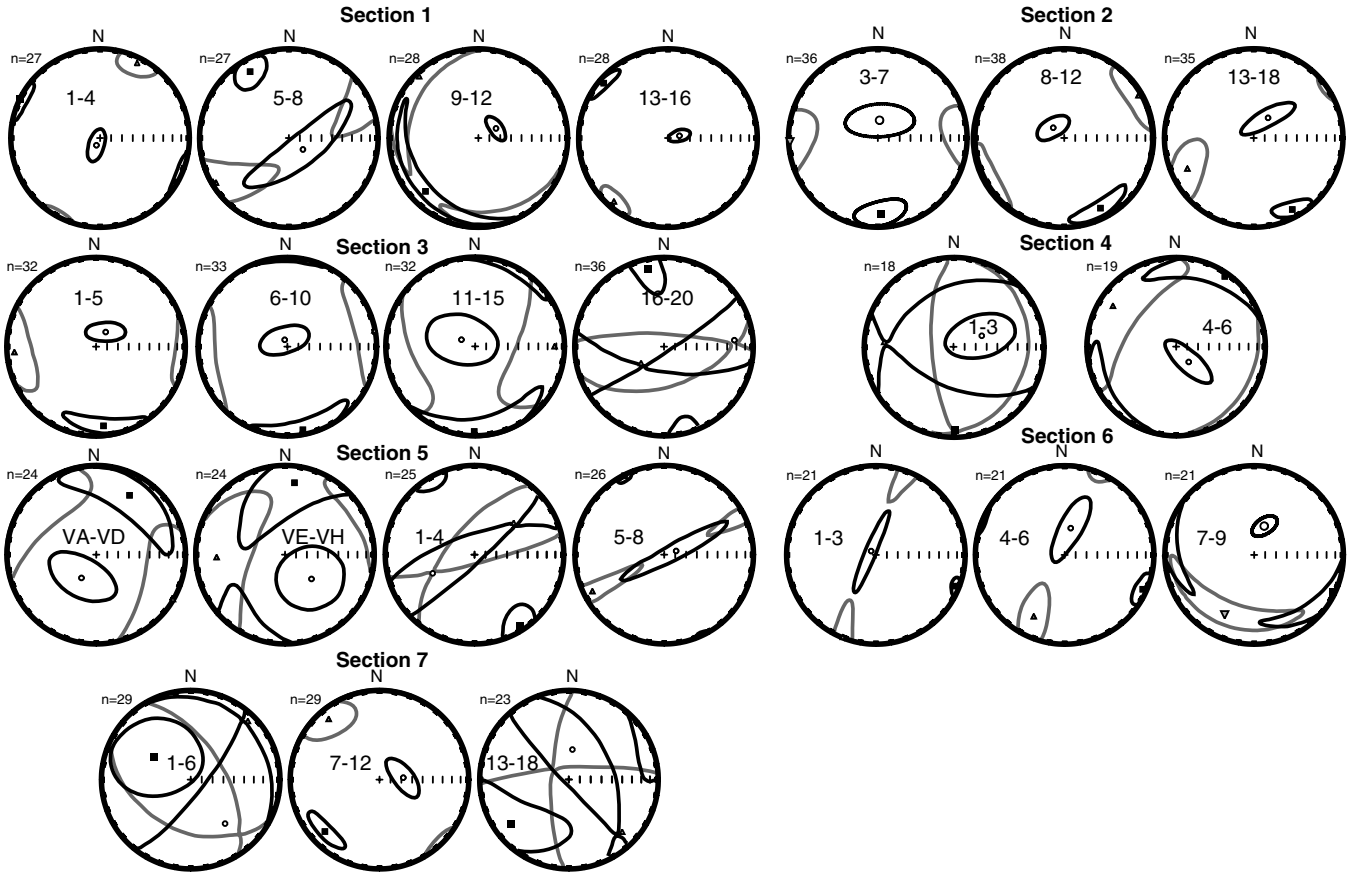

Figure 4. Successive mean principal axes and their 95 per cent confidence ellipses (Constable & Tauxe 1990) for the various flow groups considered at each section. Black squares K_{max}, grey triangles K_{int}, and white circles K_{min}. The equal-area projections are lower hemispheres in geographic coordinates.

Section 4. Moreover, flow direction can be affected by local disturbances related in particular to irregularities of the underlying flow surface. Therefore, the more samples included in the computation, the more the effects of local deviation on the mean directions are limited by averaging. Grouping of all the AMS data for each section increases the reliability of the orientation of the mean axes and of their confidence zone (Plenier *et al.* 2002; Henry *et al.* 2003).

For the sections presented in this study, no significant flow dip variations were observed on the field within the volcanic sequences. However, because several eruptive centres could be involved in the same lava pile, the mean principal axes and their 95 per cent confidence zone parameters have been calculated for groups of three to five immediately adjacent flows to check for a possible evolution of the flow direction within a section (Fig. 4). In the absence of such evolution, all data can be grouped together to infer a global flow direction. As statistical approaches are partly biased in the case of systematic axis permutations, density diagrams were also used for comparison with this global flow direction.

For Sections 2, 3 and 6, the successive groups of flow recorded an almost identical mean direction, though in the two latter sections the mean directions of the upper lava group are more scattered. For Sections 4, 5 and 7, the direction recorded from one group to another seems less consistent at the section scale, but the mean axes are not statistically different from subset to subset.

For Sections 1 and 7, the ca9-12 and fa1-6 groups of flow, respectively, differ from the other groups. However, this difference is related to the permutations of K_{max} and K_{int} allowed by the almost isotropic fabric of these groups of flow. The consistency of the mean AMS directions being verified, the AMS data of each whole section were merged.

The orientation of the mean axes obtained for each section (Table 2, Fig. 5) is very similar to that determined by flow-scale analysis when allowed. For Section 4, K_{max} scatters in an almost horizontal plane with a poorly defined SW–NE mean direction, and K_{min} is close to vertical with a confidence ellipse elongated in a plane perpendicular to K_{max}, as already observed for the other sections. Jelinek's (1981) diagrams presented in Fig. 5 display similar distributions for Sections 1, 2, 3, 5, 6 and 7, with a shape from prolate to oblate cases and a mean P' between 1.009 and 1.038. Section 4 displays the same scatter for the T parameter but only very low values for the degree of anisotropy P'.

4.3 Density diagrams

A difficulty in the statistical analysis of the AMS of volcanic flows is the possible occurrence of a permutation of the principal susceptibility axes. Such permutations, often observed, can be ascribed to (1) local strain changes (Merle 1998) owing to the palaeotopography or the position of the samples in the flow, (2) composition and size of the magnetic minerals (Rochette *et al.* 1992), (3) magnetic interactions of the grains (Grégoire *et al.* 1995), (4) rolling of the elongated particles in strong velocity gradients by analogy with sediments (Jeffery 1922; Tarling & Hrouda 1993), and (5) grain settling (Cañón Tapia *et al.* 1996). These permutations lead to perpendicular clusters for the same principal axis. This can be clearly seen using density contours on a stereonet for a large set of samples

Table 2. Summary of anisotropy of magnetic susceptibility results from the section-scale study. N is the number of samples measured. K_{mean} is the mean volume susceptibility ($\times 10^{-3}$). $\bar{s}$ is the eigenvalue of the normalized mean susceptibility tensor. Dec and Inc are the declination and the inclination of the mean susceptibility axes, respectively. E2:E1 are the semi-angles of the minor and major axes, respectively, of the 95 per cent confidence ellipse determined using the bootstrap statistic (Constable & Tauxe 1990) or the Hext-Jelinek statistic (Section 10 only). P' and T are the corrected degree of anisotropy and the shape-factor parameter respectively (Jelinek 1981). * and ** after Plenier *et al.* (2002) and Henry *et al.* (2003) respectively.

N	K_{mean}		$\bar{s}$	Dec	Inc	E2:E1	P'	T
			Section 1 (Port Christmas: 48.67°S, 69.02°E)					
110	14.7	Max	1.011	312.9	7.0	6.1/40.5	1.027	0.54
		Int	1.005	221.3	13.1	6.2/40.5		
		Min	0.985	70.5	75.1	5.7/6.2		
			Section 2 (Mont des Ruches: 48.87°S, 68.91°E)					
118	14.1	Max	1.011	157.6	12.8	6.3/11.8	1.022	−0.06
		Int	1.000	249.3	7.7	10.4/12.9		
		Min	0.990	9.7	75.0	6.2/11.7		
			Section 3 (Mont des Tempêtes: 48.88°S, 69.11°E)					
133	14.1	Max	1.009	172.1	5.1	7.7/14.3	1.016	−0.23
		Int	0.999	262.4	3.2	13.9/17.3		
		Min	0.993	24.5	84.0	8.1/17.2		
			Section 4 (Port Couvreux: 49.17°S, 69.42°E)					
37	24.4	Max	1.004	210.7	3.4	14.5/90.0	1.011	0.62
		Int	1.002	301.7	17.1	20.8/90.0		
		Min	0.994	109.8	72.6	12.9/18.1		
			Section 5 (Mont Amery: 49.29°S, 70.06°E)					
99	26.7	Max	1.009	337.3	7.1	9.6/13.3	1.016	0.17
		Int	0.999	69.1	14.1	13.5/26.4		
		Min	0.992	221.4	74.1	9.4/31.6		
			Section 6 (Port Raymond: 49.34°S, 69.80°E)					
63	41.3	Max	1.019	113.3	4.0	4.4/7.1	1.038	−0.16
		Int	0.998	204.8	20.8	7.2/11.3		
		Min	0.983	12.9	68.8	4.3/11.4		
			Section 7 (Mont Bureau: 48.97°S, 69.35°E)					
81	21.3	Max	1.005	241.2	25.3	18.0/31.3	1.009	0.03
		Int	1.000	342.3	22.3	29.6/40.9		
		Min	0.995	108.4	55.2	17.9/39.1		
			Section 9* (Mont de la Tourmente: 49.30°S, 69.39°E)					
188	32.5	Max	1.008	113.6	16.1	5.7/14.0	1.038	0.18
		Int	1.002	209.3	18.9	7.5/14.0		
		Min	0.990	345.9	64.8	5.7/7.5		
			Section 10** (Port Jeanne d'Arc: 49.57°S, 69.84°E)					
JU1 44		Max	1.008	201.0	11.0	13.3/27.4	1.016	−0.11
		Min	0.993	353.0	77.0	12.3/23.5		
JU5 108		Max	1.005	283.0	3.0	5.7/30.8	1.015	0.69
		Min	0.992	29.0	79.0	5.7/7.5		

(Rochette *et al.* 1992). Such diagrams also often allow a better estimation of the distribution symmetry relative to the vertical plane of the eigenvectors and thus can be used to infer the emplacement direction (Henry 1980; Thompson *et al.* 1986; Cañón Tapia *et al.* 1997; Cañón Tapia & Coe 2000).

Density contour plots of K_{max} and K_{min} for all the AMS data of each section (Fig. 6) are very similar for all sections: a K_{min} of high inclination and K_{max} close to the horizontal plane. The directions with the highest density of axis on the density diagrams are very similar to the global mean AMS eigenvectors of the section-scale analysis. This indicates that permutations do not significantly affect the mean tensor directions. The only exceptions are Sections 4 and 7, which display a relatively high scatter of the mean directions, probably related to their particularly low degree of anisotropy.

For the other sections, however, the minimum axes are not regularly scattered around their mean direction, but mostly spread within a strongly dipping plane, towards NNW for Sections 2 and 3, WNW for Section 6 and SSE for Sections 1 and 5. The dip direction of this plane, and thus the vertical symmetry plane of the minimum axis distribution, is then NNW–SSE or WNW–ESE according to the sections considered.

The maximum axes systematically display a bimodal distribution. Because axis permutations have been found in the same flow, these bimodal distributions are not related to flows that recorded lava emplacement from distinct eruptive centres. It is noteworthy that the

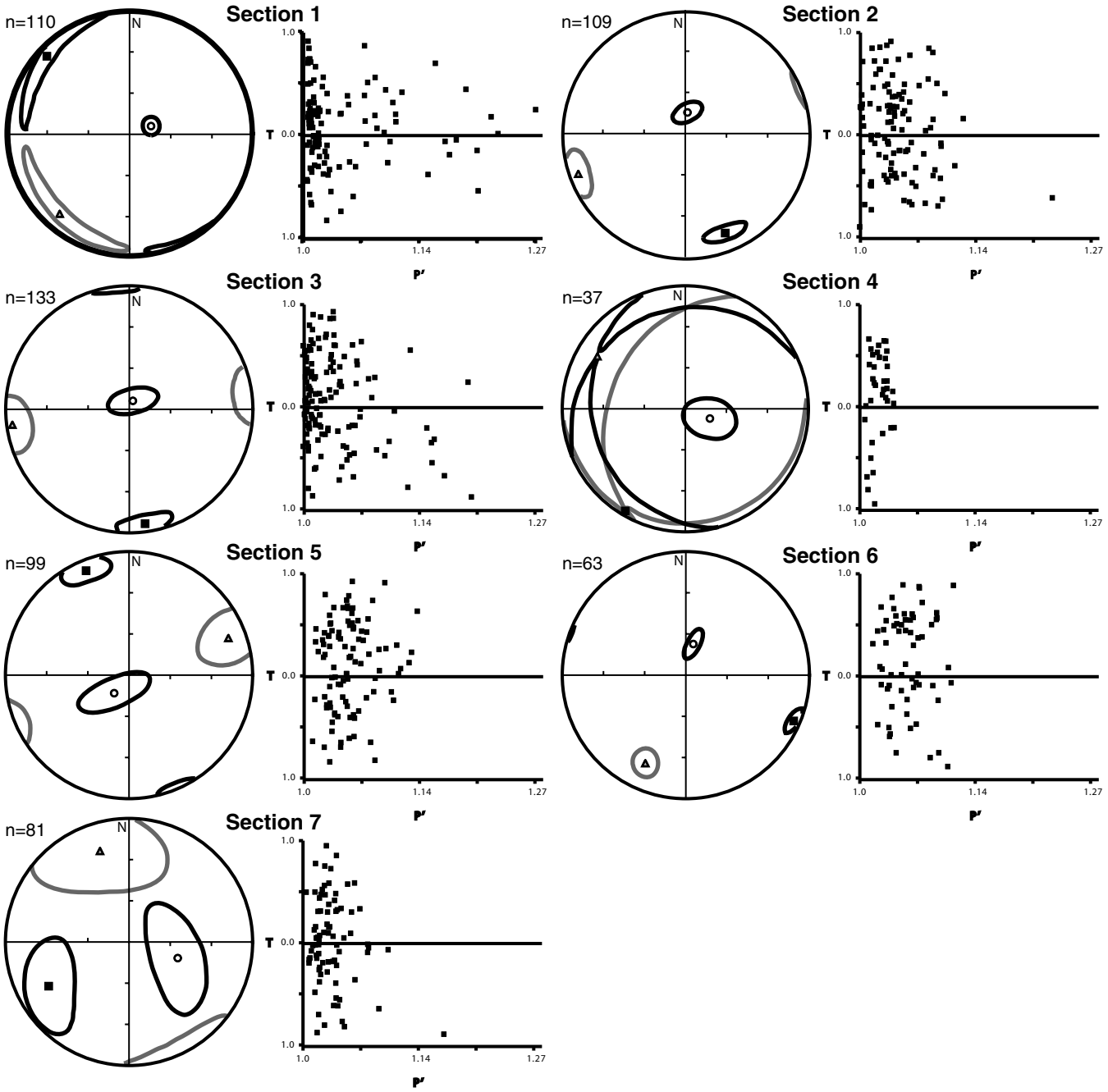

Figure 5. Section-scale analysis: mean principal axes and their 95 per cent confidence ellipses (Constable & Tauxe 1990) associated with a Jelinek plot (Jelinek 1981) for each section after merging all the data. The equal-area projections are lower hemispheres in geographic coordinates: black squares represent K_{max}, grey triangles K_{int}, and white circles K_{min}.

best-defined mean maximum axis is for Sections 1, 2, 3, 5 and 6 near the dip direction of the vertical plane indicated by the minimum axis distribution. Taken together, maximum and minimum axis distributions admit the same vertical plane of symmetry.

5 THIN-SECTION ANALYSIS

The flow directions determined using AMS have been compared to an independent flow-direction indicator (Henry 1980; Callot *et al.* 2001) represented by image analysis of thin sections.

We prepared polished thin sections parallel to the magnetic foliation plane (K_{max}–K_{int}) for two samples from Section 3 (from flows Tem16 and Tem18, Figs 7a and b, respectively) and two others from Section 5 (from flows Ame6 and Ame8, Figs 7f and g, respectively). We included in addition three other samples from a previous study (Plenier *et al.* 2002) at the Mont de la Tourmente section (from flows Tou2, Tou11 and Tou15, Figs 7c , d and e, respectively). One of these samples (Fig. 7c) has magnetic lineation (K_{max}) perpendicular to the interpreted flow direction. Obviously, two or three thin sections per lava pile are not enough to determine its emplacement direction. The aim of these analyses is only to compare discrete results from an independent method with the AMS interpretation.

Depending on the grain size, microphotographs correspond to the entire thin section or to several zoomed numeric microphotographs.

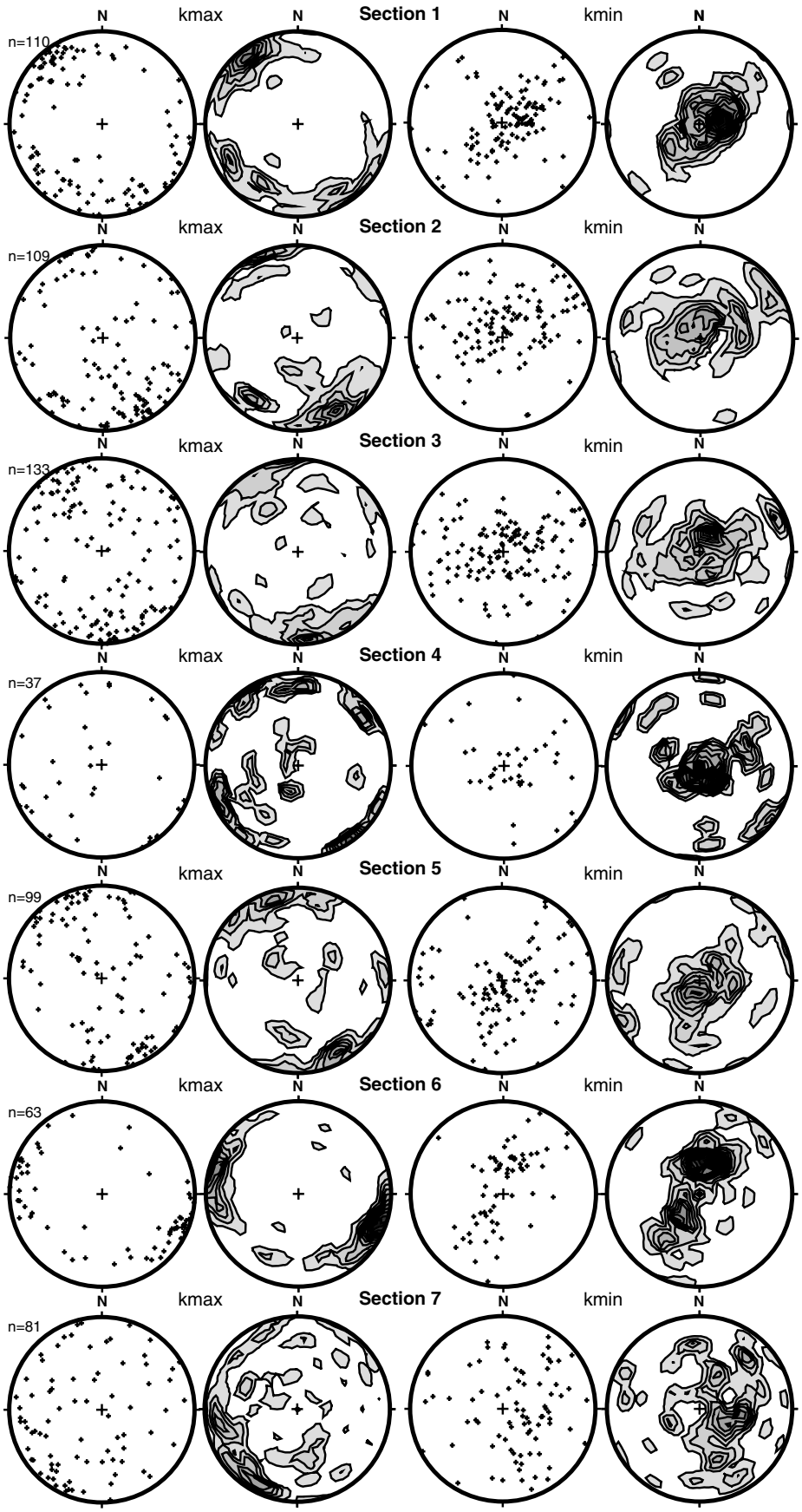

Figure 6. Horizontal (left) and vertical (right) axes associated with their density contours (stereographic projection in the lower hemisphere) for each section.

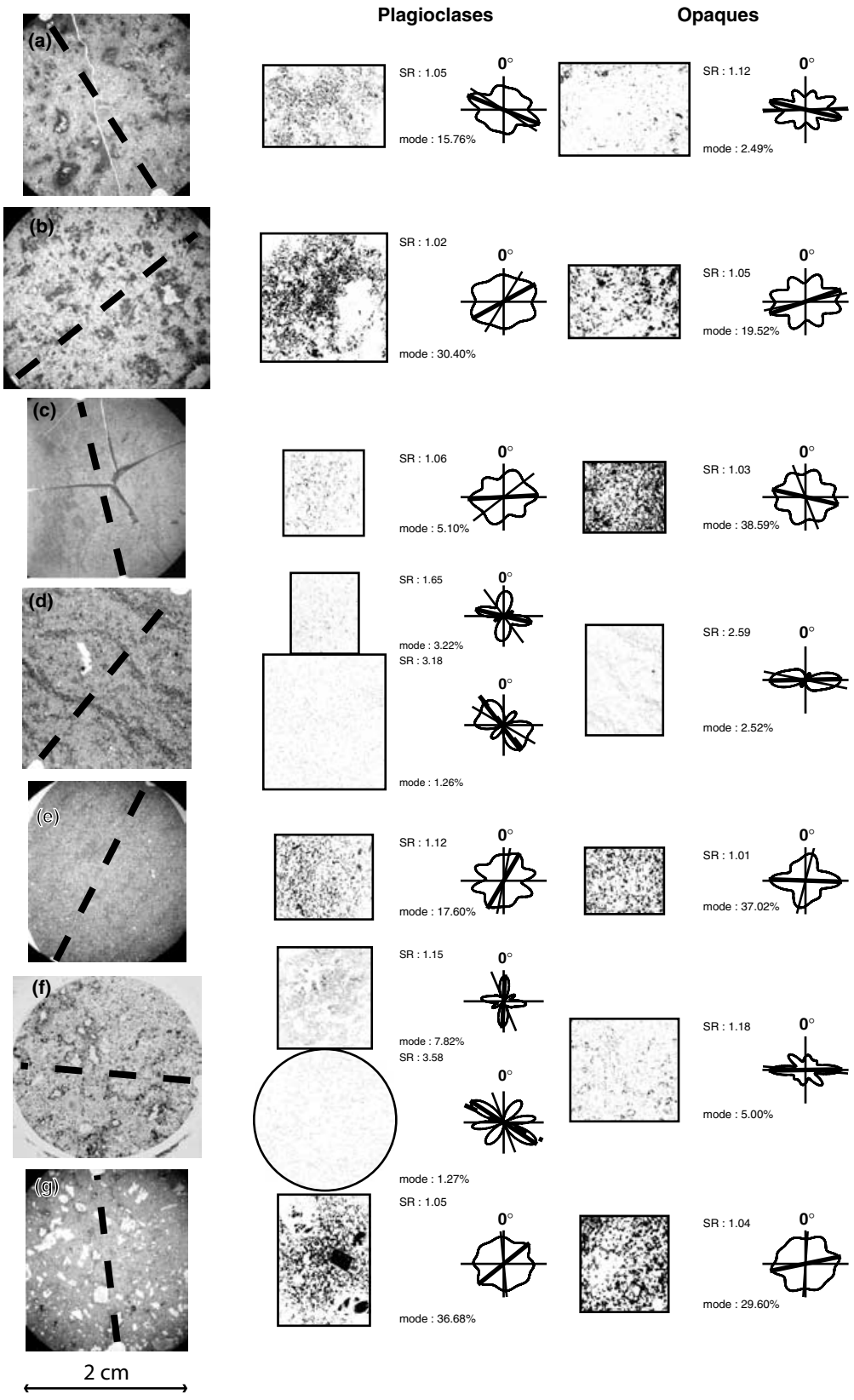

Figure 7. Shape preferential orientation (SPO) analysis of plagioclase and opaque phases: (a) and (b) show samples from Section 3; (c), (d) and (e) samples from Section 9; and (f) and (g) samples from Section 5. From left to right: global pictures of the thin section (bold dashed lines indicate the K_{max} direction), extracted black and white pictures after image filtering and their corresponding rose of direction of the plagioclase boundaries, same analysis for the opaque phase. For (d) and (f) thin sections, the redrawn plagioclase lath pictures are given at the bottom with the corresponding rose of direction diagram. For the rose diagrams, lines correspond to the long axis of the mean ellipse, bold lines are the maximum direction of the distribution, and dashed bold lines represent the mean orientation given by the method of Harvey & Laxton (1980).

After each feldspar lath had been redrawn, the cosine director method of Harvey & Laxton (1980) was initially used to determine the preferred elongation axis of the plagioclases. In the absence of imbrication and for a low velocity gradient (as expected for lava-flow emplacement on a relatively weak slope), this axis is assumed to reflect the flow direction. Unfortunately, only two thin sections show plagioclase phenocrysts. Consequently, we performed a systematic analysis using the intercept method (Launeau & Bouchez 1992), which allows random shapes to be treated (Callot *et al.* 2001). After image filtering to sharpen their bounds, the plagioclase and opaque phases were individualized in two black and white (B&W) pictures for each microphotograph. The intercept software (Launeau & Robin 1996) yielded the direction of maximum orientation of the grain boundaries, which corresponds to the preferred elongation axis of the considered phase. The coherence between the two methods has been verified for two thin sections (Figs 7d and f). Results are plotted as a rose diagram with a line indicating the sought-after preferred elongated axis of a 'mean' mineral, and a bold line corresponding to the maximum axis of the distribution. The mean orientation defined with the method of Harvey & Laxton (1980), when it was usable, is represented by a dashed bold line.

The thin sections presented in Fig. 7 display poorly anisotropic distributions of the preferred elongated axis of each phase (shape ratio SR of the order of 1.05). The maximum direction nearest to the mean orientation is thus interpreted as indicating the flow direction. Relatively good agreement between the orientation of the minerals and the magnetic lineation (dashed bold lines on the left pictures) is observed for thin sections a, b, e and g.

For sample f (Fig. 7), the contrast of colour between the plagioclase laths was not pronounced enough for them to be individualized with image filtering. The N–S maximum orientation found after analysing the filtered B&W picture supposed to correspond to the plagioclase phase then corresponds to an artefact of the digital treatment of the microphotograph. It can be due to noise introduced by the picture treatment or to the existence of several groupings of plagioclase laths together with global shapes not systematically related to the flow emplacement. Considering this problem, in that case the preferred elongated direction of the analysed phases is parallel to the magnetic lineation.

In contrast, the thin section c (Fig. 7) exhibits a maximum direction (bold line) perpendicular to the magnetic lineation (dashed bold line on the left picture) for both phases. This sample actually indicated a magnetic lineation perpendicular to the interpreted flow direction. Combined with the analysis of thin section e (Fig. 7), which shows a good agreement between the orientation of minerals and magnetic lineation, this observation confirms the emplacement direction obtained for the Mont de la Tourmente section (Plenier *et al.* 2002).

Sample d (Fig. 7) from the same section gives different results. For this thin section, K_{max} is parallel to the flow direction but the elongated axes are again perpendicular to the magnetic lineation. The flow direction deduced from this thin section should disagree with that deduced from the two other thin sections, the AMS data and the dip of the flows in the Mont de la Tourmente section. This refutes the possibility that the thin-section analysis can furnish a systematic answer for a given flow direction. However, the direction for the opaque phase clearly mimics that of the redrawn plagioclase phenocryst picture (bottom). This should suggest anisotropy of distribution of the ferromagnetic grains located along the plagioclase phenocryst boundaries (Hargraves *et al.* 1991; Callot *et al.* 2001; Ferré *et al.* 2002), giving K_{max} perpendicular to the flow direction. This does not correspond to the measured AMS, which is then probably mainly carried by very small grains, non-discernible on the picture. We can, however, observe that the B&W picture of the plagioclase phase produced from image filtering gives a bimodal distribution. This bimodality is related to the presence of plagioclases with perpendicularly oriented laths in the groundmass (not sampled in the redrawn picture) in the analysed microphotograph. A 'rolling effect' (Jeffery 1922; Tarling & Hrouda 1993), which is known to preferentially influence the phenocrysts, can be expected for a 15° dip as measured for the Mont de la Tourmente section. Hence, the secondary maximum corresponding to the groundmass is a better indicator of the flow direction. This secondary maximum direction is then in good agreement with the magnetic lineation.

6 DISCUSSION AND INTERPRETATION

6.1 Determination of the flow direction

The flow-scale analysis of the AMS data nicely defines a mean magnetic fabric for six of the sections. However, more than 50 per cent of the studied flows cannot be taken into account and consequently such an analysis of Section 4 was not possible. Grouping of all the AMS data for a section (section-scale analysis) allows each recorded datum to be considered and more confidently represents the mean flow direction of the lava piles because these statistical approaches are at least partly biased in the presence of axis permutations, the analysis of density diagrams, disregarding the intensity of the AMS directions, provides a better visualization of the distribution. Combining the three complementary approaches used in this study, two alternative flow directions can be confidently inferred for most sections: NW–SE or NE–SW for Section 1, NNW–SSE or WSW–ENE for Sections 2, 3 and 5, NNE–SSW or WNW–ESE for Section 6, and ENE–WSW or NNW–SSE for Section 7. Section 4, with only 37 samples, does not give a reliable conclusion (NW–SE or SW–NE?). Owing to the permutations of axes observed at the flow scale, there are no *a priori* reasons for the flow direction to be indicated by K_{max}. Indeed, if the majority of the samples from a given unit have a permutation of the K_{max} and K_{int} axes, the interpretation using K_{max} would lead to a 90° error in the flow-direction estimation.

When all the AMS data have been obtained in the same part of the flow (the bottom part in our case), with knowledge of the dip of the section it is theoretically possible to deduce the sense of flow by imbrication (Cañón Tapia *et al.* 1997; Cañón Tapia & Coe 2000). Then, the deviation direction of the strongly dipping mean axis from the vertical, related to imbrication, could be used to try to select the direction and sense of flow between the two possible interpretations given above for some sections. The flow should have been towards the NE for Section 1. The interpretation of flow remains ambiguous for the other sections, in particular for Section 7, which is more affected by axis permutations, displaying larger confidence ellipses and three mean directions relatively out of the horizontal plane. For Sections 2, 3, 4 and 5, the degree of imbrication is low and the interpretation made using the imbrication may not be statistically significant considering the scatter of the vertical axes. In addition, computed flow experiments (Dragoni *et al.* 1997) with rotating rigid ellipsoidal magnetite in a viscous material subjected to a velocity gradient display normal or reverse imbrication depending on the strain value for a given elongation ratio. These experiments may explain the presence of two maxima in the distribution of K_{min} for Section 6 (Fig. 6).

An alternative method for inferring a flow direction from the AMS data is to use the vertical plane of symmetry of the

distribution of susceptibility axes (Henry 1980; Thompson *et al.* 1986). Although this method cannot be used for indicating a flow sense, the vertical plane of symmetry is usually relatively well highlighted by the scatter of the K_{min} direction in the density diagrams (right part of Fig. 6). Using this alternative approach, the flow direction should have been NE–SW for Section 1, NNW–SSE or ENE–WSW for Sections 2, 3, 4, 5 and 7, and NNE-SSW or WNW–ESE for Section 6.

The determination of the symmetry of the distribution of the AMS directions is also subject to uncertainties, and there is, at this time, no reason to favour one of the two alternative interpretations. Unfortunately, analyses of thin sections are prone to the same ambiguities as in studies of AMS, because the preferred lengthening axis of minerals can be parallel or perpendicular to the flow direction. This is also apparent in the presence of several maxima on the rose distribution diagrams from thin sections. It is also interesting to note that sample d clearly has two families of opaque grains. Grains of the first type mimic the orientation of plagioclase phenocrysts and have a preferred elongated axis almost perpendicular to the flow direction, whereas AMS is mainly carried by very small grains within the groundmass with K_{max} parallel to the flow direction.

6.2 Comparison with field observations

For Sections 1, 2 and 3, several geological observations argue for a common eruptive centre located roughly west of the Loranchet Peninsula (Nougier 1970a): a shallow western submarine plateau, a global shallow dip towards the east or northeast, and a main morphology of ending flow at the eastern coast. Geomorphological observations (Nougier 1970a) show that Sections 1 to 3 belong to the same volcanic province. Their magnetic fabric is similar and the same interpretation of flow direction is therefore expected for the three sections. The NE to ENE flow sense, indicated by the clear imbrication of Section 1, is coherent with the geological observations and in good agreement with the earlier interpretation indicated in the geological map (Nougier 1970b). The northern eruptive centre should then be expected to be presently below sea level and to be located W or WSW of the Loranchet Peninsula. It is noteworthy that the scatter of the minimum axis is parallel to the interpreted flow direction. The two AMS studies previously performed on the Kerguelen Archipelago (Plenier *et al.* 2002; Henry *et al.* 2003) displayed a scatter of the minimum axis perpendicular to the interpreted flow direction. In the absence of evidence for deducing a flow direction systematically perpendicular to the scatter of the vertical axis, we decided to keep our interpretation based on geological observations. Measurements of AMS for lava flows from several localities with a flow direction independently well known would be of great interest for checking a possible systematic relationship between the scatter of the vertical axis and the flow direction.

For Section 5, another independent eruptive centre is defined in the western part of the Courbet Peninsula from clear geomorphological arguments such as the thickness variation of the lava pile. In particular, a divergence of the dip, though not very marked, from a centre located at Montagnes Vertes is described. Numerous dykes are also observed in this area. This section is thus very close to the supposed eruptive centre. For that reason, both NNW–SSE and ENE–WSW flow directions are compatible with the occurrence of an eruptive centre at Montagnes Vertes. Therefore, the sense of flow for the entire section can equally well be interpreted as SSE or WSW.

Sections 4 and 6 are located at the boundary between the Courbet Peninsula and Cook glacier volcanic provinces. Considering the consistency of the signal recorded for these sections, no mixture between two magma sources is expected. The WNW–ESE possible flow direction determined for Section 6 clearly favours an eruptive centre located in the vicinity of the Cook glacier. Moreover, this flow direction is in better agreement with the 4° dip towards the east observed at this section, and we thus interpret the flow sense as ESE. For Section 4 we interpret the flow sense as probably being from WSW to ENE, considering an eruptive centre under the Cook glacier, also in agreement with the observed dip.

Section 7 belongs to the same Cook volcanic province. A previous study (Plenier *et al.* 2002) showed that the eruption centre for another section in the same area (Section 9) was located under the Cook glacier (Nougier 1970a). Owing to a main morphology of ending flow at the eastern coast of Foch island, the same eruptive centre is strongly expected to have produced the Section 7 lava pile. The ENE flow sense that can be inferred using the imbrication for Section 7 agrees better with these observations. Keeping the same interpretation of flow sense, an eruptive centre located in the neighbourhood of the Société de géographie Peninsula cannot be totally excluded for this section.

Fig. 8 displays the supposed eruptive centre and volcanic province limits and summarizes the flow interpretation of each section. It also includes the preliminary interpretation of Section 8 (Plenier *et al.* 2004) as well as previous interpretations from two other localities (added in Table 2): Sections 9 (Plenier *et al.* 2002) and 10 (Henry *et al.* 2003). The NNE, E and NNE flow senses have been determined for Sections 8, 9 and 10, respectively, with procedures comparable to those used in this study. It is noteworthy that the emplacement sense interpreted for Section 9 is opposite to the imbrication indication. This section is close to the eruptive centre located under the Cook glacier and presents a main dip to the east. The results of this lava pile thus strongly confirm that the imbrication is not always reliable for deducing the sense of flow.

Although the lavas did not always follow a straight line during emplacement, the flow directions interpreted at each section allow the location of the corresponding eruptive centre to be refined. This is particularly true for the northern sections, which constrain the location of the eruptive centre expected by Nougier (1970a) to be in the southwestern part of the Loranchet Peninsula. The combination of the 4, 6, 8, and 9 lava-pile results confirms the location of an eruptive centre under the Cook glacier. Section 7, belonging to the same volcanic province, may equally well have its source located in the neighbourhood of the Société de géographie Peninsula. Finally, the flow in Section 10 defines an eruptive centre in the Gaby Island direction. Section 5, however, is too close to the expected Montagnes Vertes eruptive centre to be helpful in its precise location.

7 CONCLUSION

Magnetic fabric represents a reliable tool for studying emplacement conditions of lava flows. Because of an important scattering of the data, its interpretation requires the use of three different methods (statistical at flow and section scales, and the study of density contour diagrams of AMS data), and has to be based on a large number of samples. Owing to local flow deviations relative to the mean slope, the samples have to be taken in several different flows in order that the effects of these deviations can be averaged. Combining the AMS results, two alternative flow directions for each section can be confidently obtained. It is then possible to use the imbrication of the vertical axis or the symmetry of the axis distribution to choose between the two alternatives. In this study, however, these two indicators failed to confidently select between the two flow directions. Unfortunately, the shape preferential orientations of mineral phases

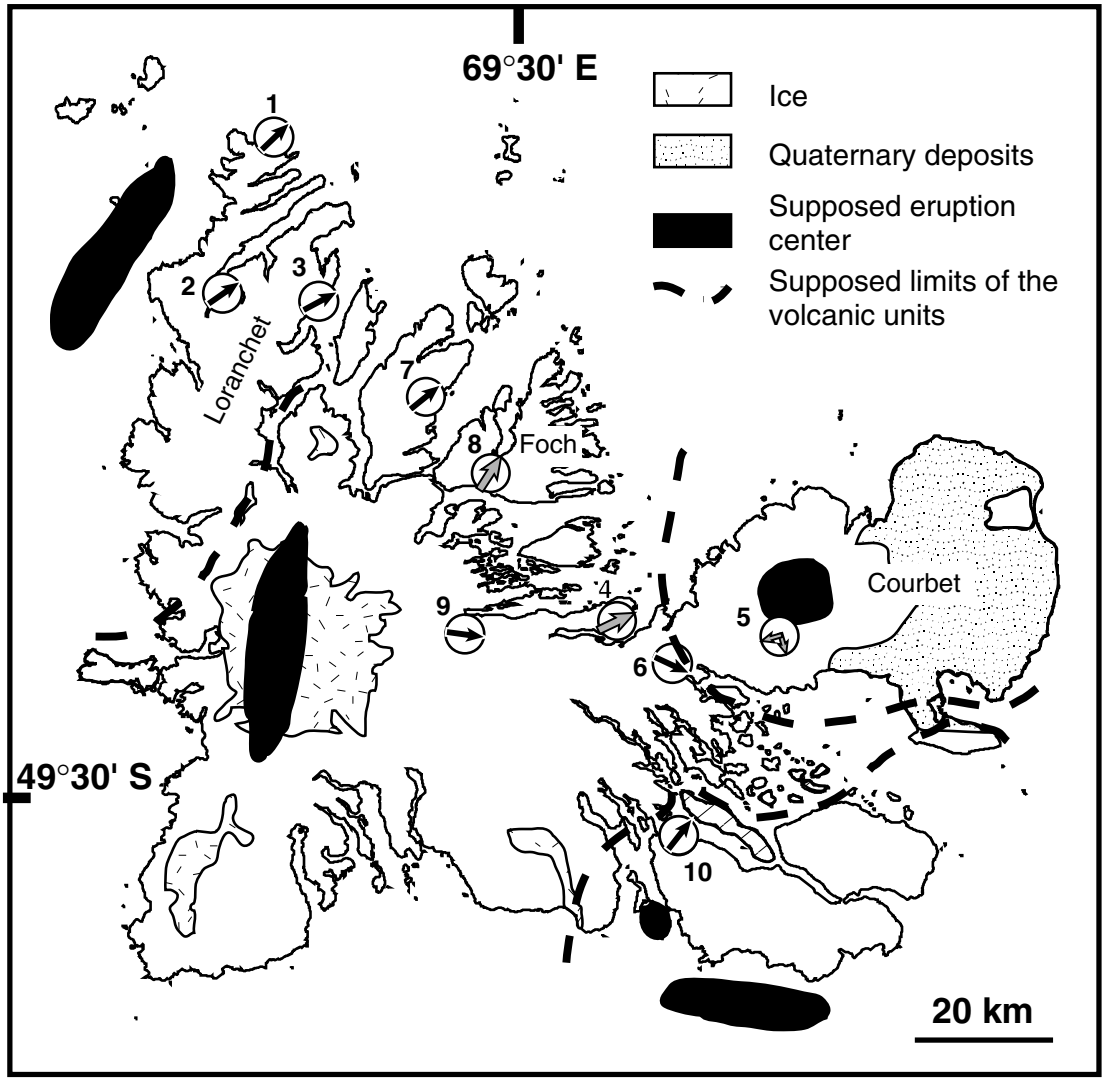

Figure 8. Summary of the interpreted flow senses of all the sections studied so far, including Sections 9 (Plenier *et al.* 2002) and 10 (Henry *et al.* 2003). The grey arrows for Sections 4, 7 (this study) and 8 (Plenier *et al.* 2004) indicate that the interpretations remain ambiguous and may vary for the latter as the analysis is not finished. The volcanic province limits (dashed bold lines) and the corresponding supposed eruptive centre location (in black) are also displayed, after Nougier (1970a) and Leyrit *et al.* (1990).

obtained from thin-section analysis are prone to the same uncertainties as the AMS data and cannot be used confidently to make a choice. Therefore, geomorphological and geological arguments were key information for specifying the direction and sense of flow. Our interpretation of emplacement sense is ENE for Sections 2, 3, 4, and 7, NE for Section 1, and ESE for Section 6. Even though the lavas may not have flowed straight from their eruptive centre during emplacement, the results of this study allow their respective sources to be located more precisely.

ACKNOWLEDGMENTS

We are grateful to the 'Institut Polaire Paul Emile Victor' for providing all transport facilities and for the support of this project. Special thanks to Alain Lamalle, Roland Pagny and all our field friends. We thank Mireille Perrin for her help during sampling, Michel Prévot for scientific discussions, Charles Aubourg for reading the first version of this manuscript and two anonymous reviewers for their helpful comments. We also thank Christophe Nevado for preparing the thin sections. This work was partially supported by CNRS-INSU Programme Intérieur Terre.

REFERENCES

Borradaile, G., 1988. Magnetic susceptibility, petrofabric and strain–a review, *Tectonophysics,* **156,** 1–20.

Borradaile, G. & Henry, B., 1997. Tectonic applications of magnetic susceptibility and its anisotropy, *Earth Sci. Rev.,* **42,** 49–93.

Bouchez, J., 2000. Magnetic susceptibility anisotropy and fabrics in granites, *C.R. Acad. Sci. Paris,* **330,** 1–14.

Cañón Tapia, E. & Coe, R., 2000. Rock magnetic evidence of inflation of a flood basalt lava flow, *Bull. Volcan.,* **64,** 289–302.

Cañón Tapia, E., Walker, G. & Herrero-Bervera, E., 1995. Magnetic fabric and flow direction in basaltic pahoehoe lava of Xitle volcano, Mexico, *J. Volc. geotherm. Res.,* **65,** 249–263.

Cañón Tapia, E., Walker, G. & Herrero-Bervera, E., 1996. The internal structure of lava flows—insights from AMS measurements I: Near-vent a'a, *J. Volc. geotherm. Res.,* **70,** 21–36.

Cañón Tapia, E., Walker, G. & Herrero-Bervera, E., 1997. The internal structure of lava flows – insights from AMS measurements II: Hawaiian pahoehoe, toothpaste lava and 'a'ā, *J. Volc. geotherm. Res.,* **76,** 19–46.

Callot, J., Geoffroy, L., Aubourg, C., Pozzi, J. & Mege, D., 2001. Magma flow directions of shallow dykes from the east greenland volcanic margin inferred from magnetic fabric studies, *Tectonophysics,* **335,** 313–329.

Constable, C. & Tauxe, L., 1990. The bootstrap for magnetic susceptibility tensors, *J. geophys. Res.,* **95,** 383, 395.

Doucet, S., Weis, D., Scoates, J., Nicolaysen, K., Frey, F. & Giret, A., 2002. The depleted mantle component in Kerguelen Archipelago basalts: Petrogenesis of tholeiitic-transitional basalts from the Loranchet Peninsula, *J. Petrol.,* **43,** 1341–1366.

Dragoni, M., Lanza, R. & Tallarico, A., 1997. Magnetic anisotropy produced by magma flow: theoritical model and experimental data from Ferrer dolerite sills (Antarctica), *Geophys. J. Int.,* **128,** 230–240.

Ferré, E.C., Bordarier, C. & Marsh, J., 2002. Magma flow inferred from AMS fabrics in a layered mafic sill, Insizwa, South Africa, *Tectonophysics,* **354,** 1–23.

Frey, F., Weis, D., Yang, H.-J., Nicolaysen, K., Leyrit, H. & Giret, A., 2000. Temporal geochemical trends in Kerguelen Archipelago basalts: evidence for decreasing magma supply from the Kerguelen plume, *Chem. Geol.,* **164,** 61–80.

Geoffroy, L., Callot, J., Aubourg, C. & Moreira, M., 2002. Magnetic and plagioclase linear fabric discrepancy in dykes: a new way to define the flow vector using magnetic foliation, *Terra Nova,* **14,** 183–190.

Giret, A., 1986. Géologie des Terres Australes Françaises, *Comité National Français Recherches Antarctique,* **58,** 17–41.

Giret, A., 1990. Typology, evolution, and origin of the Kerguelen plutonic series, Indian ocean: a review, *Geol. J.,* **25,** 239–247.

Glen, J., Renne, P., Milner, S. & Coe, R., 1997. Magma flow inferred from anisotropy of magnetic susceptibility in the coastal Paranà-Etendeka igneous province: Evidence for rifting before flood volcanism, *Geology,* **25,** 1131–1134.

Grégoire, V., de Saint Blanquat, M., Nédélec, A. & Bouchez, J., 1995. Shape anisotropy versus magnetic interactions of magnetite grains: experiments and application to AMS in granitic rocks, *Geophys. Res. Lett.,* **22,** 2765–2768.

Hargraves, R., Johnson, D. & Chan, C., 1991. Distribution anisotropy: The cause of AMS in igneous rocks?, *Geophys. Res. Lett.,* **18,** 2193–2196.

Harvey, P. & Laxton, P., 1980. The estimation of finite strain from the orientation distribution of passively deformed linear markers: eigenvalue relationships, *Tectonophysics,* **70,** 285–307.

Henry, B., 1980. Contribution à l'étude des propriétés magnétiques de roches magmatiques des Alpes: Consequences structurales, régionales et générales, *PhD thesis,* University of Paris.

Henry, B. & Plessard, C., 1997. New palaeomagnetic results from the Kerguelen Islands, *Geophys. J. Int.,* **128,** 73–83.

Henry, B., Plenier, G. & Camps, P., 2003. Post-emplacement titlting of lava flows inferred from magnetic fabric study: the example of Oligocene lavas in the Jeanne d'Arc Peninsula (Kerguelen Islands), *J. Volc. geotherm. Res.,* **127,** 153–164.

Herrero-Bervera, E., Cañón Tapia, E., Walker, G. & Tanaka, H., 2002. Magnetic fabrics study and inferred flow directions of lavas of the Old Pali Road, O'ahu, Hawaii, *J. Volc. geotherm. Res.,* **118,** 161–171.

Hext, G., 1963. The estimation of second-order tensors, with related tests and designs, *Biometrika,* **50,** 353–373.

Hrouda, F., 1982. Magnetic anisotropy of rocks and its application in geology and geophysics, *Geophys. Surv.,* **5,** 37–82.

Jeffery, G., 1922. The motion of ellipsoidal particles immersed in a viscous fluid, *Proc. R. Soc. Lond.,* **102,** 161–179.

Jelinek, V., 1978. Statistical processing of magnetic susceptibility measured in groups of specimens, *Stud. Geophys. Geod.,* **22,** 50–62.

Jelinek, V., 1981. Characterization of the magnetic fabric of rocks, *Tectonophysics,* **79,** T63–T67.

Knight, M. & Walker, G., 1988. Magma flow directions in flows of the Koolau Complex, Oahu, determined from magnetic fabric studies, *J. geophys. Res.,* **93,** 4308–4319.

Kolofikova, O., 1976. Geological interpretation of measurement of magnetic properties of basalts on example of the chribsky les lava flow of the Veljy Roudny volcano (Nizky Jesenik Mts.), *Cas. Mineral. Geol.,* **21,** 387–396 (in Czech.).

Launeau, P. & Bouchez, J., 1992. Mode et orientation préférentielle de forme des granites par analyse d'images numériques, *Bull. Soc. géol. France,* **163,** 721–732.

Launeau, P. & Robin, P., 1996. Fabric analysis using the intercept method, *Tectonophysics,* **267,** 91–119.

Leyrit, H., Bardintzeff, J., Verdier, O., Giret, A. & Brousse, R., 1990. Les presqu'îles Jeanne d'Arc et Ronarc'h: zone test pour une cartographie géologique au 1/100 000 des îles Kerguelen, *Compt. Rend. Acad. Sci. Paris,* **311,** 561–566.

Lienert, B., 1991. Monte Carlo simulation of errors in the anisotropy of magnetic susceptibility: a second-rank symmetric tensor, *J. geophys. Res.,* **96,** 19 539–19 544.

Merle, O., 1998. Internal strain within lava flows from analogue modelling, *J. Volc. Ggeotherm. Res.,* **81,** 189–206.

Morris, A., 2000. Magnetic fabric and palaeomagnetic analyses of the Plio-Quaternary calc-alkaline series of Aegina Island, South Aegean volcanic arc, Greece, *Earth planet. Sci. Lett.,* **176,** 91–105.

Nicolaysen, K., Frey, F., Hodges, K., Weis, D. & Giret, A., 2000. $^{40}Ar/^{39}Ar$ geochronology of flood basalts from the Kerguelen Archipelago, southern Indian Ocean: implications for Cenozoic eruption rates of the Kerguelen plume, *Earth planet. Sci. Lett.,* **174,** 313–328.

Nougier, J., 1970a. Contribution a l'étude géologique et géomorphologique des îles Kerguelen, *C.N.F.R.A.,* **27,** 2 tomes.

Nougier, J., 1970b. *Terres Australes et Antarctique Françaises (T.A.A.F.), Kerguelen Islands reconnaissance map,* 1:200 000, *Instit. Geograph. Nat.*, Paris.

Plenier, G., Camps, P., Henry, B. & Nicolaysen, K., 2002. Palaeomagnetic study of Oligocene (24–30 Ma) lava flows from the Kerguelen Archipelago (southern Indian Ocean): directional analysis and magnetostratigraphy, *Phys. Earth planet. Inter.,* **133,** 127–146.

Plenier, G., Camps, P., Coe, R. & Perrin, M., 2003. Absolute palaeointensity of Oligocene (24–30 Ma) lava flows from the Kerguelen Archipelago (southern Indian Ocean), *Geophys. J. Int.,* **154,** 877–890.

Plenier, G., Bascou, J., Gattacceca, J., Camps, P., Henry, B. & Rochette, P., 2003. An example of inverse magnetic fabric in a lava pile from the Kerguelen Archipelago (southern Indian Ocean), *EOS Trans. AGU,* Fall Meet. Suppl. Abstract.

Rochette, P., Jackson, M. & Aubourg, C., 1992. Rock magnetism and the interpretation of anisotropy of magnetic susceptibility, *Rev. Geophys.,* **30,** 209–226.

Tarling, D. & Hrouda, F., 1993. *The Magnetic Anisotropy of Rocks,* Chapman and Hall, London.

Tauxe, L., Gee, J. & Staudigel, H., 1998. Flow directions in dykes from AMS data: The bootstrap way, *J. geophys. Res.,* **103,** 17 775–17 790.

Thompson, J., Guillaume, A. & Daly, L., 1986. Paleomagnetism of the Permian volcanic rocks of Moissey (French Jura): implications for the paleofield and tectonic evolution, *Geophys. J. R. astr. Soc.,* **86,** 103–117.

Ventura, G., 2001. The strain path and emplacement mechanism of lava flows: an example from Salina (southern Tyrrhenian Sea, Italy), *Earth planet. Sci. Lett.,* **188,** 229–240.

Weis, D. & Giret, A., 1994. Kerguelen plutonic complexes: Sr, nd, pb isotopic study and inferences about their sources, age and geodynamic setting, *Mem. Soc. Géol. Fr.,* **166,** 47–59.

Weis, D., Damasceno, D., Frey, F., Nicolaysen, K. & Giret, A., 1998. Temporal isotopic variations in the Kerguelen plume: evidence from the Kerguelen Archipelago, *Miner. Mag.,* **62A,** 1643–1644.

Yang, H.-J., Frey, F., Weis, D., Giret, A., Pyle, D. & Michon, G., 1998. Petrogenesis of the flood basalts forming the northern Kerguelen Archipelago: Implications for the Kerguelen plume, *J. Petrol.,* **39**, 711–748.

Zhu, R., Shi, C. & Liu, Q., 2003. Anisotropy of magnetic susceptibility of Hannuoba basalt, northern China: Constraints on the vent position of the lava sequences, *Geophys. Res. Lett.,* **30,** 1066, doi:10.1029/2002GL016215.